

## Dynamic Phase Alignment in Navier-Stokes Turbulence

Lucio M. Milanese<sup>\*</sup> and Nuno F. Loureiro<sup>†</sup>

*Plasma Science and Fusion Center, Massachusetts Institute of Technology, Cambridge, Massachusetts 02139, USA*

Stanislav Boldyrev<sup>‡</sup>

*Department of Physics, University of Wisconsin-Madison, Madison, Wisconsin 53706, USA  
and Space Science Institute, Boulder, Colorado 80301, USA*



(Received 28 April 2021; accepted 4 November 2021; published 30 December 2021)

In Navier-Stokes turbulence, energy and helicity injected at large scales are subject to a joint direct cascade, with both quantities exhibiting a spectral scaling  $\propto k^{-5/3}$ . We demonstrate via direct numerical simulations that the two cascades are compatible due to the existence of a strong scale-dependent phase alignment between velocity and vorticity fluctuations, with the phase alignment angle scaling as  $\cos \alpha_k \propto k^{-1}$ .

DOI: [10.1103/PhysRevLett.127.274501](https://doi.org/10.1103/PhysRevLett.127.274501)

**Introduction.**—The incompressible Navier-Stokes equations (NSEs) govern the dynamics of a broad variety of physical systems [1]. Many of these systems are in a turbulent state: they exhibit chaotic dynamics which cannot be readily described from first principles, but is instead partially captured by phenomenological and statistical models [2]. The prominent Kolmogorov cascade model [3] captures key aspects of fluid turbulent dynamics based on the assumption that, in three-dimensional systems, the kinetic energy of the turbulent fluctuations is transferred from larger to smaller-scale structures via nonlinear interactions that are local in wave number  $k$ .

Kolmogorov’s theory of turbulence was developed considering energy as the only nonlinear invariant of the system. It was subsequently discovered [4,5], however, that a second inviscid invariant of the incompressible NSEs exists, namely, the helicity, defined as  $\mathcal{H} = \int \mathbf{v} \cdot \boldsymbol{\omega} dV$ , with  $\mathbf{v}$  the velocity of the fluid and  $\boldsymbol{\omega} = \nabla \times \mathbf{v}$  its vorticity. A flow with net helicity is necessarily more complex than otherwise, as its mirror symmetry is broken [6].

The existence of a second nonlinear invariant further complicates the analysis of the turbulent dynamics. In principle, it is possible for both invariants to cascade forward, i.e., from large to small scales, or for them to cascade in different directions [7,8]. When both quantities cascade forward, it is in principle possible for either invariant to set the (scale-dependent) amplitude of velocity fluctuations, thus affecting the nonlinear eddy turnover time and leading to different predictions [7,9]. Indeed, the helicity density at scale  $\lambda$  can be dimensionally evaluated as  $H_\lambda \sim v_\lambda \omega_\lambda \sim v_\lambda^2 / \lambda$ , and the nonlinear interaction time (eddy turnover time) as  $\tau_\lambda \sim \lambda / v_\lambda$ , where  $v_\lambda$  and  $\omega_\lambda$  denote the typical amplitudes of velocity and vorticity fluctuations at scale  $\lambda$ . Assuming the existence of a constant helicity flux, i.e.,  $\varepsilon_H \sim H_\lambda / \tau_\lambda \sim \text{const}$ , one would derive  $v_\lambda \propto \lambda^{2/3}$ , and

the resulting energy and helicity spectra would be, respectively,  $\mathcal{E}(k) \propto k^{-7/3}$  and  $\mathcal{H}(k) \propto k^{-4/3}$  [9]. This scenario leads to a scaling of the energy spectrum different from Kolmogorov’s  $\mathcal{E}(k) \propto k^{-5/3}$ , which is instead defined by a constant energy flux,  $\varepsilon \sim v_\lambda^2 / \tau_\lambda$ , and the corresponding velocity scaling  $v_\lambda \propto \lambda^{1/3}$ . In this case, dimensional arguments would predict the spectral scaling of helicity to be  $\mathcal{H}(k) \propto k^{-2/3}$ . However, this “naïve” estimate of the helicity spectrum is, as we discuss below, inconsistent with a constant helicity flux in the inertial range.

In many instances, the simultaneous presence of two invariants in a turbulent system requires that one conserved quantity cascades to small scales, while the other one cascades to large scales. Such a phenomenon was discovered by Kraichnan in pioneering work on two-dimensional turbulence [10], and later studied more broadly in various models of weak and strong turbulence [11–13]. In the case of Navier-Stokes turbulence, the naïve dimensional arguments suggest that it is the helicity invariant that should exhibit the direct cascade, while the energy should inverse cascade. Indeed, a cascade of energy to small scales,  $\varepsilon = \text{const}$ , would seem to imply the divergence of the helicity flux,  $\varepsilon_H \sim \varepsilon / \lambda$  at small scales, contradicting helicity conservation. Similarly, if helicity cascaded to large scales,  $\varepsilon_H = \text{const}$ , then the energy flux  $\varepsilon \sim \lambda \varepsilon_H$  would diverge at large scales, contradicting energy conservation. The only possibility of maintaining a steady state would be, therefore, to assume a direct cascade for helicity and inverse for energy.

This is not, however, what occurs in three-dimensional Navier-Stokes turbulence, where instead *both* energy and helicity are observed to cascade forward. Theoretical arguments in favor of the existence of a joint direct cascade of the two invariants in the presence of net helicity were first put forward in Ref. [9], based on conservation of

energy and helicity in the inertial range, and in Ref. [14], based on the analysis of inviscid statistical equilibria. There exists today significant experimental and numerical evidence that energy and helicity in Navier-Stokes turbulence are indeed both subject to a direct cascade [6–8,15–18], and share a spectral scaling of  $\propto k^{-5/3}$ . While the double direct cascade of energy and helicity has been the subject of robust investigation and seems beyond reasonable doubt [6,18–38], the turbulent mechanism that enables it has remained unclear.

The goal of this Letter is to uncover such a mechanism. We argue that this joint cascade is possible because the velocity and vorticity fluctuations develop a progressively stronger *phase correlation* at smaller scales. More precisely, we propose that while the energy flux is dimensionally evaluated as  $\varepsilon \sim v_\lambda^2/\tau_\lambda$ , the helicity flux should be evaluated as

$$\varepsilon_H \sim r_\lambda v_\lambda \omega_\lambda / \tau_\lambda \sim r_\lambda v_\lambda^2 / (\lambda \tau_\lambda), \quad (1)$$

where  $r_\lambda$  is a scale-dependent cancellation factor. Assuming that the (scale-dependent) nonlinear time  $\tau_\lambda$  is determined purely by the energy cascade, and requiring that both the energy and helicity fluxes be constant in the inertial range, allows one to predict the scaling of the cancellation factor:

$$r_\lambda \sim \lambda/L, \quad (2)$$

where  $L$  is the outer scale of the turbulence.

When the cancellation factor is present, the simultaneous direct cascade of *both* energy and helicity becomes possible, and one predicts the scaling  $\mathcal{H}(k) \propto k^{-5/3}$  for the helicity spectrum. In this Letter we argue that the cancellation factor underpinning the spectral scaling of helicity is a manifestation of *dynamic phase alignment*, i.e., a scale-dependent correlation between the fluctuations of velocity and vorticity, and demonstrate this result by means of direct numerical simulations of driven, incompressible Navier-Stokes turbulence.

*Numerical setup.*—We integrate the NSEs numerically with the pseudospectral code `Tarang` [39,40] on a cubic, triply periodic domain using a grid of  $N^3$  collocation points. The “2/3’s rule” is used for dealiasing [39]. The model equations read

$$\frac{\partial \mathbf{v}}{\partial t} + \mathbf{v} \cdot \nabla \mathbf{v} = -\nabla P + \nu \nabla^2 \mathbf{v} + \mathbf{F}, \quad (3)$$

coupled to the incompressibility condition,  $\nabla \cdot \mathbf{v} = 0$ .  $P$  is the pressure,  $\nu$  is the kinematic viscosity and  $\mathbf{F}$  represents external forcing. Both  $P$  and  $\mathbf{F}$  are normalized to the fluid density, set as  $\rho \equiv 1$ . The pressure is computed by solving a Poisson equation obtained by taking the divergence of Eq. (3) and using the incompressibility condition. In all simulations, energy and helicity are injected at wave numbers  $2 \leq |\mathbf{k}_f| \leq 6$ . Wave numbers are normalized to

the size of the simulation domain, so that the smallest wave number, which represents box-scale fluctuations, has value unity. We define the energy and helicity injection rates, respectively, as

$$\varepsilon_E = \sum_{\mathbf{k}_f} \Re \{ \mathbf{F}(\mathbf{k}) \cdot \mathbf{v}^*(\mathbf{k}) \}, \quad (4)$$

$$\varepsilon_H = \frac{1}{2} \sum_{\mathbf{k}_f} \Re \{ \mathbf{F}(\mathbf{k}) \cdot \boldsymbol{\omega}^*(\mathbf{k}) - \mathbf{v}(\mathbf{k}) \cdot [i\mathbf{k} \times \mathbf{F}(\mathbf{k})] \}, \quad (5)$$

where  $\mathbf{F}(\mathbf{k})$  represents the delta-correlated in time forcing term, and  $\Re$  denotes the real part. The forcing algorithm is described in detail in Ref. [36]. We further define the ratio of helicity to energy injection as  $\mathcal{R}_H = \varepsilon_H / \bar{k} \varepsilon_E$ , where  $\bar{k} = \sum_{\mathbf{k}_f} |\mathbf{k}| F(\mathbf{k}) / \sum_{\mathbf{k}_f} F(\mathbf{k})$  is the weight-averaged wave number of the forcing.

Table I summarizes key parameters of the simulations performed. We define the Reynolds number as  $\text{Re} = v_{\text{rms}} L / \nu$ , where  $L = \int_0^\infty k^{-1} \mathcal{E}(k) dk / \int_0^\infty \mathcal{E}(k) dk$  is the integral length scale of the turbulence and  $v_{\text{rms}} = \sqrt{2\mathcal{E}/3}$  is the root mean square of the velocity fluctuations. The inverse of the Kolmogorov scale is represented by  $k_d = (\nu^3/\varepsilon_E)^{-1/4}$ .

*Dynamic phase alignment.*—The net helicity density at each wave number is a function of the absolute value of the Fourier coefficients  $|v_k|$  and  $|\omega_k|$ , and of the phase angle between them,  $\alpha_k$ . At a given wave number  $k$ , the average value of  $\alpha_k$  is given by

$$\cos \alpha_k = \frac{1}{2} \sum_i \frac{\langle v_{i_k} \omega_{i_k}^* + \text{c.c.} \rangle}{\langle |v_{i_k}| |\omega_{i_k}| \rangle}, \quad (6)$$

where  $\langle \dots \rangle$  represents averaging over the wave number shell and we are summing over the index  $i \in \{x, y, z\}$  representing the three spatial directions. We can write the spectral scaling of helicity as  $\mathcal{H}(k) \sim k^{-1} v_\lambda \omega_\lambda \cos \alpha_k \sim k^{-2/3} \cos \alpha_k$ , where the last step is obtained under the assumptions  $v_\lambda \sim k^{-1/3}$  and  $\omega_\lambda \sim k^{2/3}$ . Conservation of helicity in the direct cascade requires a scaling  $\mathcal{H}(k) \sim k^{-5/3}$ . We thus predict a scaling  $\cos \alpha_k \sim k^{-1}$ .

In Figs. 1(a)–1(c), we show the energy and helicity spectra (from time-averaged data in steady state) for simulations A1–A3. Good agreement with the scaling  $\propto k^{-5/3}$  is recovered for both invariants. The product of

TABLE I. Summary of key simulation parameters.

ID	N	Re	$\mathcal{R}_H$	$k_d$
A1	1024	1350	0.1	150
A2	1024	1350	0.3	150
A3	1536	2000	0.5	205

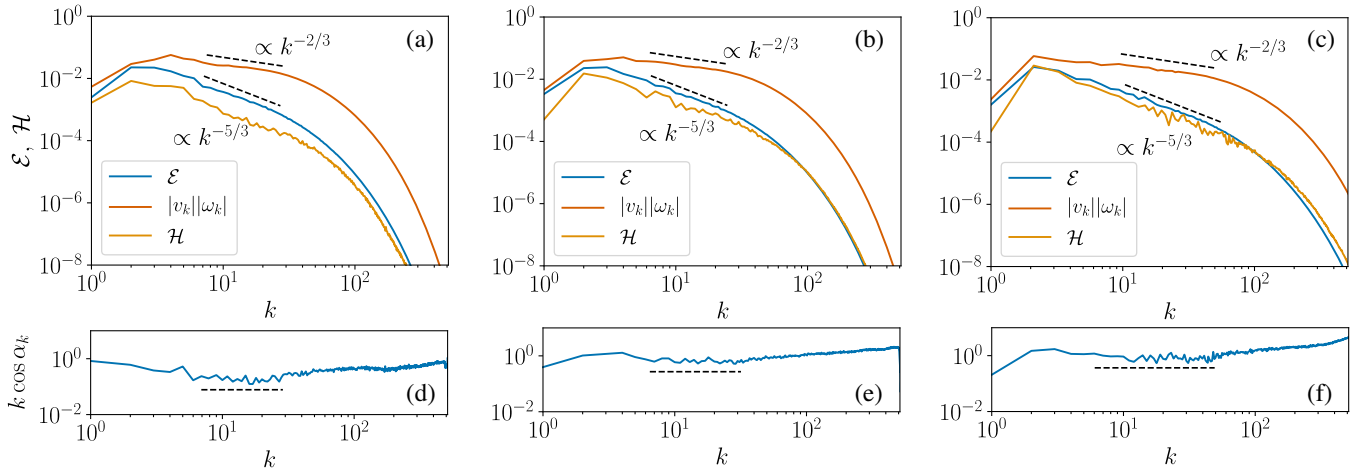


FIG. 1. Subplots (a),(b),(c) show spectra of energy, helicity, and the product of the absolute value of velocity and vorticity for simulations A1–A3, respectively. Subplots (d),(e),(f) present compensated spectra of the average value of the cosine of the phase angle [Eq. (6)] between velocity and vorticity fluctuations. The inertial range covers wave numbers up to  $k \approx 35$  (for simulations A1 and A2) and up to  $k \approx 50$  (for A3), after which dissipation becomes non-negligible and the predicted scalings do not apply.

the absolute value of velocity and vorticity [the denominator of the right-hand side in Eq. (6)] exhibits good agreement with the spectral scaling  $\propto k^{-2/3}$ , predicted via dimensional arguments. Figures 1(d)–1(f) show compensated spectra of the phase alignment angle between fluctuations of velocity and vorticity as function of scale, demonstrating that it follows a scaling  $\cos \alpha_k \propto k^{-1}$  in the inertial range. The plots in Fig. 1 demonstrate that the scaling  $\cos \alpha_k \propto k^{-1}$  occurs for a broad range of ratios of helicity to energy injection in the system. An investigation of the Reynolds number dependence of these results is reported in the Supplemental Material [41].

When  $\cos \alpha_k = 0$ , helicity is zero and the system is mirror symmetric. The scaling  $\cos \alpha_k \propto k^{-1}$  therefore implies that dynamic phase alignment underpins the restoration of mirror symmetry at small scales, in agreement with simulations of Navier-Stokes turbulence where net helicity is injected at large scales [6–8].

*Absence of geometric angle alignment.*—We argued above that the reduction of helicity was associated with phase alignment, that is, scale-dependent cancellation of positive and negative values of the product  $\mathbf{v} \cdot \boldsymbol{\omega}$ . However, a scale-dependent *angular* alignment between the directions of the fields may also, in principle, constitute the *primary* mechanism of helicity reduction. In order to investigate the possible existence of such an angular alignment, we consider the band-pass filtered velocity and vorticity fields. The band-pass filtered velocity is defined as  $\mathbf{v}_\ell = \mathcal{F}^{-1}(\hat{\mathbf{v}})$ , where  $\mathcal{F}^{-1}$  denotes the inverse Fourier transform, while  $\hat{\mathbf{v}}$  denotes the field after undergoing Gaussian filtering of the form  $\exp\{-(k - k_c)^2/2\sigma^2\}$ , with  $k_c^{-1} \equiv \ell$  and  $\sigma = 3$ . The band-pass filtered vorticity field is defined as  $\boldsymbol{\omega}_\ell = \nabla \times \mathbf{v}_\ell$  [42]. We will demonstrate numerically that their phase and angular correlations disentangle statistically, and that, in contrast with phase

alignment, geometric angular alignment does not exhibit scale dependence. Consider first two scalar fields,  $X$  and  $Y$ , that may stand for, e.g., the  $x$  components of the velocity and vorticity vectors. Assume that we may represent them as  $X = X_0 \cos \phi$  and  $Y = Y_0 \cos(\phi + \phi_0)$ , where  $X_0$  and  $Y_0$  are positive amplitudes,  $\phi$  is a random phase, and  $\phi_0$  is the phase shift. The correlation between these fields is given by  $\langle XY \rangle = (1/2)X_0Y_0 \cos \phi_0$ . Similarly, one can calculate the correlation between the normalized fields,  $X/|X|$  and  $Y/|Y|$ . The product of these fields can only take two values,  $+1$  or  $-1$ , with the corresponding probabilities depending on the phase shift,  $P_+ = 1 - (\phi_0/\pi)$  and  $P_- = \phi_0/\pi$ . It is convenient to denote the deviation of the phase shift from  $\pi/2$  as  $\tilde{\phi}_0 = \pi/2 - \phi_0$ , so that the probabilities take the form  $P_+ = 1/2 + \tilde{\phi}_0/\pi$  and  $P_- = 1/2 - \tilde{\phi}_0/\pi$ . Then, the correlation function of the normalized fields is

$$\left\langle \frac{X}{|X|} \frac{Y}{|Y|} \right\rangle = P_+ - P_- = \frac{2\tilde{\phi}_0}{\pi}. \quad (7)$$

We now turn to the vector fields  $\mathbf{v}_\ell$  and  $\boldsymbol{\omega}_\ell$ . In order to study their phase and geometric correlations, consider the product  $Z = \mathbf{v}_\ell \cdot \boldsymbol{\omega}_\ell / |\mathbf{v}_\ell| |\boldsymbol{\omega}_\ell|$ . Clearly, we can represent it as  $Z = \xi |\cos \theta|$ , where the “phase” variable  $\xi$  takes the values  $\pm 1$ , while  $\theta$  is the geometric angle between the directions of the fields. The statistics of  $Z$  are given by the joint probability density function  $p(\xi, |\cos \theta|)$ :

$$P(\xi, |\cos \theta|) = P\left(\xi \middle| |\cos \theta|\right) P(|\cos \theta|). \quad (8)$$

The probability density of the variable  $Z$  is then

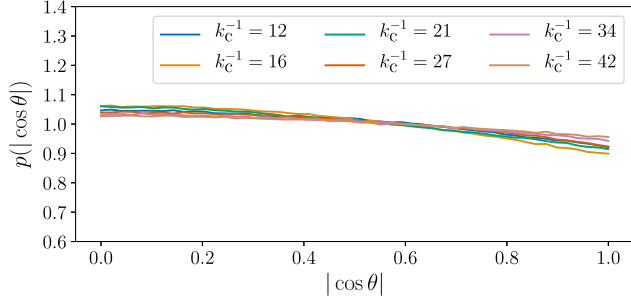


FIG. 2. Probability density function of the absolute value of the geometric angle between band-pass-filtered fluctuations of velocity and vorticity. No significant dependence on scale is observed. Data obtained from simulation A3.

$$p(Z) = \begin{cases} p(+1|\cos\theta)p(|\cos\theta|), & Z > 0, \\ p(-1|\cos\theta)p(|\cos\theta|), & Z < 0, \end{cases} \quad (9)$$

where, in the right-hand side, one needs to substitute  $\cos\theta = Z$ . By analogy with the scalar case, we may identify the difference of the conditional probabilities with the phase shift between the fluctuating vector fields evaluated at a given geometric angle:

$$p(+1|\cos\theta) - p(-1|\cos\theta) = \frac{2\tilde{\phi}_0}{\pi} \Big|_{|\cos\theta|}. \quad (10)$$

The remaining probability density,  $p(|\cos\theta|)$ , describes their geometric correlation.

Using the probability density function in Eq. (9), we may now average the  $Z$  field:

$$\langle Z \rangle = \int_0^1 \left( \frac{2\tilde{\phi}_0}{\pi} \Big|_{|\cos\theta|} \right) p(|\cos\theta|) \cos\theta d(\cos\theta). \quad (11)$$

The first term in the integrand describes the contribution from the phase alignment between the velocity and vorticity fields, while the second term,  $p(|\cos\theta|)$ , describes the contribution from their geometric alignment. In principle, both terms may depend on the filtering scale  $\ell$ . Our numerical simulations, however, demonstrate that, quite crucially, the scale dependence factors out in the first term; that is,

$$\frac{2\tilde{\phi}_0}{\pi} \Big|_{|\cos\theta|} \approx a_\ell g(|\cos\theta|) \approx a_\ell |\cos\theta|, \quad (12)$$

while the probability density of the geometric angle,  $p(|\cos(\theta)|)$ , turns out to be virtually independent of the scale. Figures 2 and 3, obtained from time-averaged data from simulation A3, show that indeed the functions  $p(|\cos\theta|)$  and  $g(|\cos\theta|)$  do not vary with scale, while the phase-alignment function scales as  $a_\ell \sim \ell \sim k^{-1}$ , in agreement with the

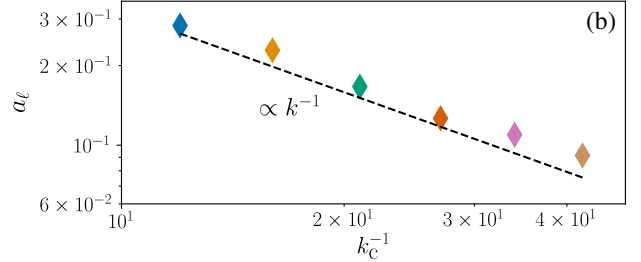
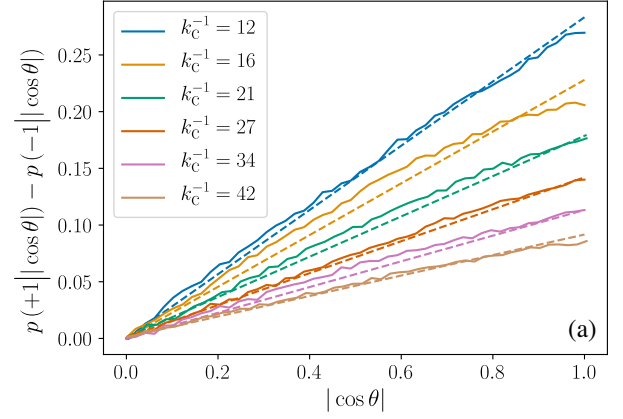


FIG. 3. (a) Difference between conditional probability of positive and negative alignment for a given  $|\cos\theta|$  (solid lines) and linear fit of the data for each wave number range (dashed lines). The figure illustrates that, at each scale, the function  $g(|\cos\theta|)$  is well approximated by a linear expression, i.e.,  $g(|\cos\theta|) \approx |\cos\theta|$ . (b) Slope coefficients of the linear fits  $a_\ell$  for the different wave number ranges. The color coding highlights the correspondence between data presented in subplots (a) and (b). Data obtained from simulation A3.

Fourier-space analysis of the previous section. These conclusions hold for other values of  $\mathcal{R}_\mathcal{H}$ . As shown in Fig. 3(a),  $g(|\cos\theta|)$  is well approximated by a linear function, i.e.,  $g(|\cos\theta|) \approx |\cos\theta|$ , for all wave number ranges, with  $a_\ell$  representing the slope of the linear fit at each scale [Fig. 3(b)]. Our analysis demonstrates that it is phase alignment, not geometric alignment, that determines the scale-dependent reduction of helicity, so that

$$\langle Z \rangle \approx C a_\ell \sim C a_0 \ell / \ell_0, \quad (13)$$

where we used  $a_\ell \sim a_0(\ell/\ell_0)$ , with  $\ell_0$  the outer scale of turbulence,  $a_0$  a constant dependent on net helicity in the system, and  $C$  a scale-independent constant,

$$C = \int_0^1 g(|\cos\theta|) p(|\cos\theta|) \cos\theta d(\cos\theta) \approx 1/3, \quad (14)$$

where the last approximate equality can be obtained for  $g(|\cos\theta|) \approx |\cos\theta|$  and  $p(|\cos\theta|) \approx 1$ .

*Discussion and conclusions.*—In this Letter, we demonstrate that the direct cascades of energy and helicity in Navier-Stokes turbulence can coexist because of a scale



dependence of the average Fourier phase angle between the fluctuations of velocity and vorticity. This behavior, termed dynamic phase alignment, constitutes an essential mechanism for such joint direct cascade because the scalings  $v_\lambda \sim k^{-1/3}$  and  $\omega_\lambda \sim kv_\lambda$  are preserved in the presence of net helicity. We can write the helicity spectral scaling as  $\mathcal{H}(k) \sim k^{-1}v_\lambda\omega_\lambda \cos \alpha_k \sim k^{-2/3} \cos \alpha_k$ . Deviations from  $\mathcal{H}(k) \sim k^{-2/3}$  are underpinned by a dependence on scale of  $\cos \alpha_k$ , allowing energy and helicity to cascade forward while preserving conservation of both invariants. We show that the observed spectrum  $\mathcal{H}(k) \sim k^{-5/3}$  results from the scaling  $\cos \alpha_k \propto k^{-1}$ , which underlies the progressive balancing of turbulence (restoration of mirror symmetry) in the inertial range. We also demonstrate that there exists no significant scale-dependent *geometric* alignment between velocity and vorticity, supporting our conclusion that *phase* alignment is the primary mechanism contributing to the scale-dependent reduction of helicity. In Ref. [45], it was found that dynamic phase alignment between the fluctuations of electric and magnetic potentials underpins the joint forward cascade of energy and generalized kinetic helicity in a range of anisotropic turbulent plasma systems. This remarkable similarity between systems governed by different sets of equations is suggestive of a powerful unifying paradigm, whereby the conservation of energy and a second invariant in a joint cascade determines the scale-dependent phase alignment between the two fields in the integrand of the second invariant. Dynamic phase alignment thus acquires importance as a mechanism regulating the dynamics in the presence of two invariants, arising from their conservation in the joint direct cascade, regardless of the details of the physical interactions.

While we provided significant evidence for the existence and importance of dynamic phase alignment, we stopped short of characterizing how it emerges from the nonlinear interactions. Dynamic phase alignment need not be regarded as necessarily alternative to other proposed paradigms for characterizing imbalanced turbulence [6,7,19,38,46–51]. As an example, Ref. [19] explains the spectral scaling of helicity as arising from an imbalanced transfer between modes of positive and negative chirality within the helical decomposition framework [52]. It is possible that dynamic phase alignment results from such transfer.

Work supported by DOE Grant No. DE-FG02-91ER54109 (L. M. M. and N. F. L.), NSF CAREER Grant No. PHY-1654168 (N. F. L.), the Professor Amar G. Bose Research Fellows Program at MIT (L. M. M. and N. F. L.), the Manson Benedict Fellowship of the MIT Nuclear Science and Engineering Department (L. M. M.), and NSF Grants No. PHY-1707272 and PHY-2010098, NASA Grant No. 80NSSC18K0646, and DOE Grant No. DESC0018266 (S. B.). We thank S. Chatterjee, A. Teimurazov, S. Sadhukhan, M. K. Sharma, R. Samtaney,

and M. Verma of the Tarang collaboration for support and helpful discussions. This research used resources of the facilities of the Massachusetts Green High-Performance Computing Center (MGHPCC) and of the National Energy Research Scientific Computing Center (NERSC), a U.S. Department of Energy Office of Science User Facility operated under Contract No. DE-AC02-05CH11231. We thank Z. Zhao of the NERSC staff for outstanding technical support.

---

\*milanese@mit.edu

- [1] C. Foias, O. Manley, R. Rosa, and R. Temam, *Encyclopedia of Mathematics and its Applications* (Cambridge University Press, Cambridge, England, 2001).
- [2] U. Frisch, *Turbulence* (Cambridge University Press, Cambridge, England, 1995).
- [3] A. N. Kolmogorov, The local structure of isotropic turbulence in an incompressible viscous fluid for very large Reynolds number, *Dokl. Akad. nauk SSSR* **30**, 299 (1941).
- [4] J. J. Moreau, Constantes d'un flot tourbillonnaire en fluide parfait barotrope, *C.R. Hebd. Seances Acad. Sci.* **252**, 2810 (1961), <https://hal.archives-ouvertes.fr/hal-01865239/document>.
- [5] H. K. Moffatt, The degree of knottedness of tangled vortex lines, *J. Fluid Mech.* **35**, 117 (1969).
- [6] Q. Chen, S. Chen, G. L. Eyink, and D. D. Holm, Intermittency in the Joint Cascade of Energy and Helicity, *Phys. Rev. Lett.* **90**, 214503 (2003).
- [7] A. Alexakis and L. Biferale, Cascades and transitions in turbulent flows, *Phys. Rep.* **767–769**, 1 (2018).
- [8] A. Pouquet, D. Rosenberg, J. E. Stawarz, and R. Marino, Helicity dynamics, inverse, and bidirectional cascades in fluid and magnetohydrodynamic turbulence: A brief review, *Earth Space Sci.* **6**, 351 (2019).
- [9] A. Brissaud, U. Frisch, J. Léorat, M. Lesieur, and A. Mazure, Helicity cascades in fully developed isotropic turbulence, *Phys. Fluids* **16**, 1366 (1973).
- [10] R. H. Kraichnan, Inertial ranges in two-dimensional turbulence, *Phys. Fluids* **10**, 1417 (1967).
- [11] U. Frisch, A. Pouquet, J. Léorat, and A. Mazure, Possibility of an inverse cascade of magnetic helicity in magnetohydrodynamic turbulence, *J. Fluid Mech.* **68**, 769 (1975).
- [12] A. Hasegawa, Self-organization processes in continuous media, *Adv. Phys.* **34**, 1 (1985).
- [13] V. E. Zakharov, V. S. Lvov, and G. Falkovich, *Statistical Description of Weak Wave Turbulence* Springer Series in Nonlinear Dynamics (Springer Berlin Heidelberg, Berlin, Heidelberg, 1992).
- [14] R. H. Kraichnan, Helical turbulence and absolute equilibrium, *J. Fluid Mech.* **59**, 745 (1973).
- [15] V. Borue and S. A. Orszag, Spectra in helical three-dimensional homogeneous isotropic turbulence, *Phys. Rev. E* **55**, 7005 (1997).
- [16] B. M. Koprov, V. M. Koprov, V. M. Ponomarev, and O. G. Chkhetiani, Experimental studies of turbulent helicity and its spectrum in the atmospheric boundary layer, *Dokl. Phys.* **50**, 419 (2005).

- [17] B. Qu, A. Naso, and W. J. Bos, Cascades of energy and helicity in axisymmetric turbulence, *Phys. Rev. Fluids* **3**, 014607 (2018).
- [18] F. Plunian, A. Teimurazov, R. Stepanov, and M. K. Verma, Inverse cascade of energy in helical turbulence, *J. Fluid Mech.* **895**, A13 (2020).
- [19] Q. Chen, S. Chen, and G. L. Eyink, The joint cascade of energy and helicity in three-dimensional turbulence, *Phys. Fluids* **15**, 361 (2003).
- [20] G. L. Eyink, Locality of turbulent cascades, *Physica (Amsterdam)* **207D**, 91 (2005).
- [21] J. Baerenzung, H. Politano, Y. Ponty, and A. Pouquet, Spectral modeling of turbulent flows and the role of helicity, *Phys. Rev. E* **77**, 046303 (2008).
- [22] R. A. Stepanov, P. G. Frik, and A. V. Shestakov, Spectral properties of helical turbulence, *Fluid Dyn.* **44**, 658 (2009).
- [23] Y. Choi, B.-G. Kim, and C. Lee, Alignment of velocity and vorticity and the intermittent distribution of helicity in isotropic turbulence, *Phys. Rev. E* **80**, 017301 (2009).
- [24] T. Teitelbaum and P. D. Mininni, Effect of Helicity and Rotation on the Free Decay of Turbulent Flows, *Phys. Rev. Lett.* **103**, 014501 (2009).
- [25] F. Plunian, T. Lessinnes, D. Carati, and R. Stepanov, Helicity scalings, *J. Phys. Conf. Ser.* **318**, 042013 (2011).
- [26] A. Pouquet, A. Sen, D. Rosenberg, P. D. Mininni, and J. Baerenzung, Inverse cascades in turbulence and the case of rotating flows, *Phys. Scr.* **T155**, 014032 (2013).
- [27] L. Biferale, S. Musacchio, and F. Toschi, Split energy-helicity cascades in three-dimensional homogeneous and isotropic turbulence, *J. Fluid Mech.* **730**, 309 (2013).
- [28] E. B. Gledzer and O. G. Chkhetiani, Inverse energy cascade in developed turbulence at the breaking of the symmetry of helical modes, *JETP Lett.* **102**, 465 (2015).
- [29] M. De Pietro, L. Biferale, and A. A. Mailybaev, Inverse energy cascade in nonlocal helical shell models of turbulence, *Phys. Rev. E* **92**, 043021 (2015).
- [30] G. Sahoo, F. Bonaccorso, and L. Biferale, Role of helicity for large- and small-scale turbulent fluctuations, *Phys. Rev. E* **92**, 051002(R) (2015).
- [31] R. Stepanov, E. Golbraikh, P. Frick, and A. Shestakov, Hindered Energy Cascade in Highly Helical Isotropic Turbulence, *Phys. Rev. Lett.* **115**, 234501 (2015).
- [32] P. R. Imazio and P. D. Mininni, Passive scalars: Mixing, diffusion, and intermittency in helical and nonhelical rotating turbulence, *Phys. Rev. E* **95**, 033103 (2017).
- [33] G. Sahoo, M. De Pietro, and L. Biferale, Helicity statistics in homogeneous and isotropic turbulence and turbulence models, *Phys. Rev. Fluids* **2**, 024601 (2017).
- [34] O. G. Chkhetiani and E. B. Gledzer, Helical turbulence with small-scale energy and helicity sources and external intermediate scale noises as the origin of large scale generation, *Physica (Amsterdam)* **486A**, 416 (2017).
- [35] A. Briard, L. Biferale, and T. Gomez, Closure theory for the split energy-helicity cascades in homogeneous isotropic homochiral turbulence, *Phys. Rev. Fluids* **2**, 102602(R) (2017).
- [36] A. S. Teimurazov, R. A. Stepanov, M. K. Verma, S. Barman, A. Kumar, and S. Sadhukhan, Direct numerical simulation of homogeneous isotropic helical turbulence with the TARANG code, *J. Appl. Mech. Tech. Phys.* **59**, 1279 (2018).
- [37] G. Sahoo and L. Biferale, Energy cascade and intermittency in helically decomposed Navier-Stokes equations, *Fluid Dyn. Res.* **50**, 011420 (2018).
- [38] Z. Yan, X. Li, and C. Yu, Scale locality of helicity cascade in physical space, *Phys. Fluids* **32**, 061705 (2020).
- [39] M. K. Verma, A. Chatterjee, K. S. Reddy, R. K. Yadav, S. Paul, M. Chandra, and R. Samtaney, Benchmarking and scaling studies of pseudospectral code Tarang for turbulence simulations, *Pramana* **81**, 617 (2013).
- [40] A. G. Chatterjee, M. K. Verma, A. Kumar, R. Samtaney, B. Hadri, and R. Khurram, Scaling of a fast fourier transform and a pseudo-spectral fluid solver up to 196608 cores, *J. Parallel Distrib. Comput.* **113**, 77 (2018).
- [41] See Supplemental Material at <http://link.aps.org/supplemental/10.1103/PhysRevLett.127.274501> for an investigation of the dependence on Reynolds number of the results presented in this Letter.
- [42] We use Fourier band-pass filtering to determine  $v_\ell$  and  $\omega_\ell$  because, as is well-known [33,43,44], two-point structure functions of vorticity are heavily influenced by small-scale fluctuations and thus cannot be reliably used to compare different scales in the inertial range.
- [43] E. Ott, Y. Du, K. R. Sreenivasan, A. Juneja, and A. K. Suri, Sign-Singular Measures: Fast Magnetic Dynamos, and High-Reynolds-Number Fluid Turbulence, *Phys. Rev. Lett.* **69**, 2654 (1992).
- [44] S. I. Vainshtein, Y. Du, and K. R. Sreenivasan, Sign-singular measure and its association with turbulent scalings, *Phys. Rev. E* **49**, R2521 (1994).
- [45] L. M. Milanese, N. F. Loureiro, M. Daschner, and S. Boldyrev, Dynamic Phase Alignment in Inertial Alfvén Turbulence, *Phys. Rev. Lett.* **125**, 265101 (2020).
- [46] Y. Li, Geometrical statistics and vortex structures in helical and nonhelical turbulences, *Phys. Fluids* **22**, 035101 (2010).
- [47] A. Alexakis, Helically decomposed turbulence, *J. Fluid Mech.* **812**, 752 (2017).
- [48] M. Linkmann, Effects of helicity on dissipation in homogeneous box turbulence, *J. Fluid Mech.* **856**, 79 (2018).
- [49] M. Buzzicotti, H. Aluie, L. Biferale, and M. Linkmann, Energy transfer in turbulence under rotation, *Phys. Rev. Fluids* **3**, 034802 (2018).
- [50] L. Biferale, K. Gustavsson, and R. Scatamacchia, Helicoidal particles in turbulent flows with multi-scale helical injection, *J. Fluid Mech.* **869**, 646 (2019).
- [51] Z. Yan, X. Li, C. Yu, J. Wang, and S. Chen, Dual channels of helicity cascade in turbulent flows, *J. Fluid Mech.* **894**, R2 (2020).
- [52] F. Waleffe, The nature of triad interactions in homogeneous turbulence, *Phys. Fluids A* **4**, 350 (1992).